UDC 539.4

Surface Effect on the Nanowire Forest Indentation

F. Yang[a,b]

[a] Department of Mechanics, Xi'an University of Science and Technology, Xi'an, China

[b] Department of Engineering Mechanics, Xi'an Jiaotong University, Xi'an, China

yangfan0832@163.com

The surface effect on the mechanical behavior of a nanowire forest indentation is theoretically studied. The use of a large-radius spherical indenter revealed a complex deformation pattern of the nanowire forest. The nanowire forest compression, buckling and postbuckling were analyzed. The effect of surface and packing density on the nanowire forest behavior with the indentation depth is discussed. The results show that the surface effect is of importance for in-depth hardness. The analysis is instrumental in measuring the mechanical properties of the nanowire forest and in designing nanowire-forest devices for various applications.

Keywords: surface effects, nanowire forests, indentation.

Introduction. Vertically aligned nanowires and nanotubes (nanoforests) have many potential applications, such as field emission, super-hydrophobic surfaces, optoelectronics, solar cells and energy absorption materials etc [1, 2]. On vertically aligned carbon nanotube forest, a facile yet efficient route has been successfully developed to fabricate well dispersed Ni nanoparticles [3]. In addition to their electronic, optical and wetting properties, the mechanical properties of these nanoforests are important to their functional performance. For nanoforests, it is of more interest to estimate the overall statistical properties of nanowires and nanotubes rather than those of individual wires. Using flat punch nano-indentation, Maschmann et al. [4] examined the axial compressive mechanical behavior of carbon nanotube arrays. Xiao et al. [5] used electro-discharge machining with different electrode sizes to study the machining mechanism of a carbon nanotube forest. Using a sharp atomic force microscopy (AFM) tip to conduct nanoindentation into a nanoforest, Qi et al. [6] determined the collective behavior of nanotubes, in which each nanotube was modeled as a cantilever subjected to bending. When a comparatively larger-radius indenter is employed, individual nanotubes are directly compressed and then buckle upon reaching a critical load. Wang et al. [7] investigated the force-depth behavior of indentation into a nanoforest by both the finite element method and an analytical model.

It is known that the mechanical behaviors of nanowires such as their elastic modulus and yield stress etc. display strongly size dependence on its cross-sectional size. Surface effects play an important role to contribute noticeably to the mechanical behavior of nanowires, owing to the remarkably large surface area to volume ratio. For examples, Chen et al. [8] proposed a core-shell model to explain the size-dependent elastic modulus of ZnO nanowires. Miller and Shenoy [9] adopted the surface elasticity theory to analyze the stretching and bending of nanobeams, which shows a good agreement with direct atomic simulations. Wang and Feng [10, 11] studied both the impact of residual surface stress and of surface elasticity on the buckling and vibration of the nanobeams. He and Lilley [12] addressed the static bending of nanowires and proved the size dependence of the elastic modulus with this model. Qiu et al. [13] have demonstrated the rational design and fabrication of meso-/macroporous $ZnCo_2O_4/MnO_2$ hierarchical core/shell nanocone forests using a facile hydrothermal approach. Zheng et al. [14] found the effect of surface elasticity on the elastic moduli can be well characterized by the Cauchy–Born surface model.

It is noteworthy that the surface effect on the overall behavior of nanowire forest indentation has not been accounted for. Meanwhile, the post-buckling of nanowire forests has not been considered during the indentation process in many indentation studies, despite the fact that it often occurs and has great research significance in the indentation test.

Hence, the objective of the current work is to study the effects of surface elasticity and residual surface stress on the mechanics of indentation into nanowire forests. During the whole indentation process, the complicated deformation behavior of nanowire forests with the large spherical indenter in this analysis includes compression, buckling and post-buckling.

The paper is organized as follows. In Section 2, we address surface effects on the deformation of a single nanowire under compression. Based on the force-displacement relationship of a nanowire that we obtain, the indentation of nanoforest is then analyzed in Section 3.

1. Deformation of a Nanowire under Compression. During the indentation of nanowire forests, each nanowire under the indenter experiences linearly elastic compression, buckling, and post-buckling. As a preparation, we first analyze the influence of surface effects on the deformation of a single nanowire. Surface effects on the mechanical response of nano-structured elements can be considered for using surface stresses σ^s. In accordance with the assumption of Cammarate [15], the relation between surface stresses σ^s and strain tensor ε in a one-dimensional linear model is given by

$$\sigma^s = \tau^0 + E^s \varepsilon, \tag{1}$$

where τ^0 is the residual surface stress, while E^s is the surface elastic modulus, which can be obtained through atomistic simulations or experiments [9].

When surface effects are considered, the effective flexural rigidity $(EJ)^*$ of a nanowire is given by [10, 11]

$$(EI)^* = \begin{cases} \dfrac{1}{12} Ebt^3 + \dfrac{1}{2} E^s bt^2 + \dfrac{1}{6} E^s t^3 & \text{(rectangular)}, \\ \dfrac{\pi}{64} ED^4 + \dfrac{\pi}{8} E^s D^3 & \text{(circular)}, \end{cases} \tag{2}$$

and the effective stiffness $(EA)^*$ is [9]

$$(EA)^* = \begin{cases} Ebt + 2E^s (b+t) & \text{(rectangular)}, \\ \dfrac{\pi}{4} ED^2 + E^s \pi D & \text{(circular)}, \end{cases} \tag{3}$$

where b is the width and t is the height for a rectangular cross section while D is the diameter of a circular cross section, and E is the bulk elastic modulus of the nanowire.

Based on the Laplace–Young equation, the influence of residual surface stress is described by a distributed normal pressure q_n depending on the current surface curvature κ:

$$q_n = H^* \kappa, \tag{4}$$

where H^* expresses a constant determined by the residual surface stress and the cross-sectional shape

$$H^* = \begin{cases} 2\tau^0 b & \text{(rectangular)}, \\ 2\tau^0 D & \text{(circular)}. \end{cases} \tag{5}$$

In the process of compression, when the axial load is less than the critical load, the nanowire experiences a pure elastic compression, while the compression force is related to the end displacement h by

$$P = (EA)^* h/l, \tag{6}$$

where l is the length of nanowire.

When the axial load P reaches the critical value P_{cr}, the nanowire may buckle. With the account of the surface effect, the critical load for a fixed-hinged beam is given by

$$P_{cr} = \frac{2\pi^2 (EI)^*}{l^2} + H^*. \tag{7}$$

For a fixed-free nanowire, the critical load is derived implicitly as in [16],

$$H^* = P_{cr} \cos\left(\sqrt{\frac{P_{cr} - H^*}{(EI)^*}}\, l \right). \tag{8}$$

Meanwhile, for the conventional Euler beam the critical axial load is

$$P_{cr}^0 = \frac{\eta\pi^2 (EI)_0}{l^2}, \tag{9}$$

with $\eta = 2$ for a fixed-hinged beam, $\eta = 1/4$ for a cantilever beam, and

$$(EI)_0 = \begin{cases} \dfrac{1}{12} Ebt^3 & \text{(rectangular)}, \\ \dfrac{\pi}{64} ED^4 & \text{(circular)}. \end{cases} \tag{10}$$

When the compression load is beyond the critical value P_{cr}, postbuckling takes place. It is necessary to employ the finite deformation to determine the force displacement relationship. For convenience, the arc length s and the slope angle θ are denoted in the deformation of an nanowire. The displacements along the axial and transverse directions of the nanowire are used by $u(x)$ and $w(x)$. Denoting ds/dx as Λ, the geometric equations can be expressed as

$$\frac{du}{dx} = \Lambda\cos\theta - 1, \qquad \frac{dw}{dx} = \Lambda\sin\theta, \qquad \frac{d\theta}{dx} = \Lambda\frac{d\theta}{ds}. \tag{11}$$

The curvature κ of the deformed central axis and the strain of central axis ε_0 are given by

$$\varepsilon_0 = \Lambda - 1, \qquad \kappa = -\frac{d\theta}{ds}. \tag{12}$$

Consequently, the moment M and the axial resultant force N of the same cross section are obtained as

$$M = (EI)^* \kappa, \qquad N = (EA)^* \varepsilon_0, \tag{13}$$

where $(EA)^*$ and $(EI)^*$ are derived via Eqs. (2) and (3), respectively.

For a differential element of length ds between two cross sections normal to the deflected axis of the beam, the equilibrium conditions yield:

$$\frac{dH}{ds} = q_n \sin\theta, \qquad \frac{dV}{ds} = q_n \cos\theta, \qquad \frac{dM}{ds} = H\sin\theta + V\cos\theta, \tag{14}$$

where H is the component of the resultant force along the x-axis and V is the components of the resultant force along y-axis. Using H and V, the axial resultant force N can be gives

$$N = V\sin\theta - H\cos\theta. \tag{15}$$

Considering the differential equations (11) and (14) with specified boundary conditions, shooting method is employed to solve the two-point boundary value problem numerically.

To illustrate surface effects on the compression of nanowires, we consider a silver nanowire with $E = 76$ GPa, $\tau^0 = 0.89$ J/m^2, and $E^s = 1.22$ N/m [17]. For nanowires with circular cross section of radius D and $l = 200$ nm, Fig. 1 displays the force–displacement relationship for a fixed-hinged and a fixed-free nanowires, respectively. According to the conventional elastic analysis, the normalized load P/P_{cr}^0 expresses independent of the absolute size of beam D. However, when surface effects are involved, the normalized axial load P/P_{cr}^0 depends evidently on the diameter D, especially when D reduces to dozens of nanometers.

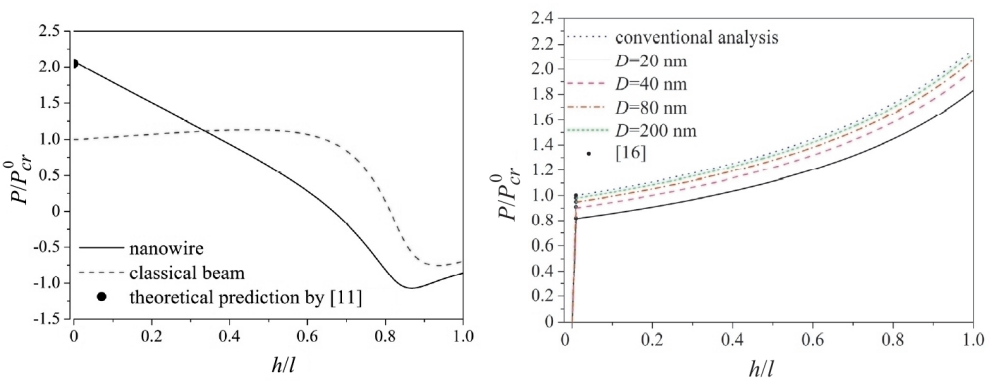

Fig. 1. The applied load vs the displacement of a nanowire for the fixed-hinged (a) and cantilever (b) cases.

It is seen that surface effects enhance the critical load for a fixed-hinged nanowire, while the axial force will decrease after buckling. Conversely, surface effects decrease the critical load for a cantilever, while it needs to increase the axial force for further compression. It is noticed that for $h/l < 0.3$, the force displacement relationship can be described by a uniform expression for both cases as

$$P/P_{cr}^{0} = \begin{cases} \alpha h/h_{cr}, & h < h_{cr}, \\ \alpha[1+\beta(\beta-\varepsilon_{cr})], & h \geq h_{cr}, \end{cases} \tag{16}$$

where $\alpha = P_{cr}/P_{cr}^{0}$, $\beta = h/l$, $\varepsilon_{cr} = P_{cr}/(EA)^{*}$, $h_{cr} = \varepsilon_{cr} l$.

Thus the influence of surface effects on the force displacement relationship is completely reflected by two factors α and β. Figure 1 plots the dependence of α and β on the diameter D of nanowires.

2. Analytical Indentation into Nanowire Forests Model. Now, we consider the indentation on nanowire forests with a spherical indenter as illustrated in Fig. 2. Assume each nanowire has the same length l, and the radius R of the indenter is much larger than l. For a simplification, we neglect the intermolecular interaction between nanowires, and we assume that the nanowire contacts the indenter only at its top end after post-buckling, which can be ensured for $h/l < 0.3$.

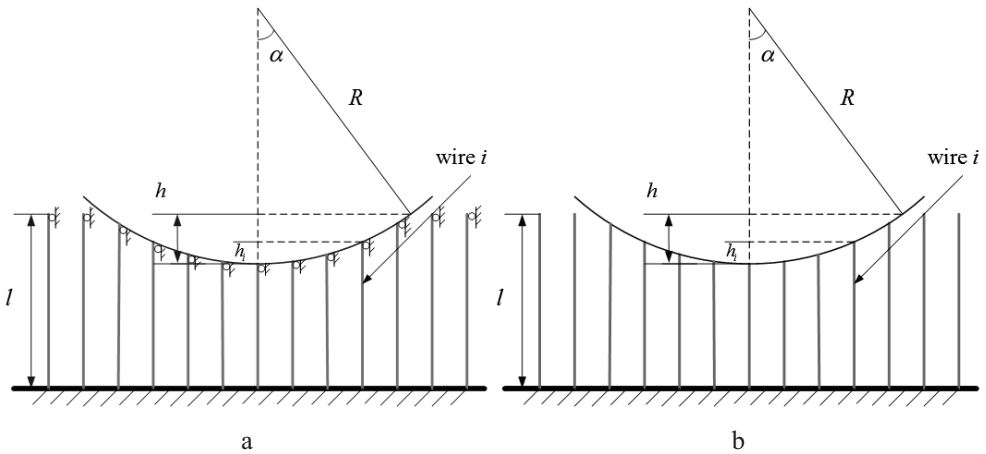

Fig. 2. Schematic of indentation on nanowire forests.

The friction between the indenter and the nanowires affects the critical buckling load of an individual tube. We consider two extreme cases. When the indenter/nanowire interface is frictionless, the nanowires are modeled by fixed-free beams. When the indenter/nanowire interface is completely rough, and no slip is permitted, the nanowires are simulated by clamped-pinned beams.

When the indent depth $h < h_{cr}$, nanowires under the indenter experience a pure compression:

$$P = \sum_{i=1}^{n} P_i, \tag{17}$$

where n is the number of nanowires encountering the indenter and P_i is the indentation force for the ith individual nanowire and its magnitude is determined by its indentation depth h_i in terms of Eq. (6).

Assuming a uniform distribution of nanowires with m nanowires per unit area, then the total indentation force is obtained by

$$P = \int_0^h P_{cr}\left(\frac{h-h_i}{l}\right) 2m\pi(R-h_i)\,dh_i = m\pi l^2 P_{cr}\varepsilon_{cr}\left(\frac{h}{h_{cr}}\right)^2\left(\frac{R}{l}-\frac{h}{3l}\right). \tag{18}$$

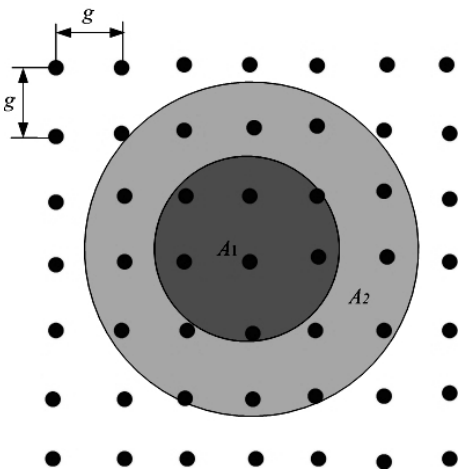

Fig. 3. Schematic of penetration area on nanowire forests.

When the indent depth $h > h_{cr}$, parts of nanowires around the indenter tip will take place buckling as indicated by the penetration area A_1 (Fig. 3), while parts of nanowires around the contact fringe are still under simple compression. The boundary between them is determined by $h_i = h_{cr}$. Thus, the resultant force P is transferred to nanowires under postbuckling in area A_1 and nanowires under elastic compression in area A_2.

Then,

$$F = P_1 + P_2 = \sum_{A_1} p_i + \sum_{A_2} p_i , \tag{19}$$

$$P_1 = \int_0^{(h-h_{cr})} p_{cr}\left(1+\beta\frac{h-h_i}{l}\right)2m\pi(R-h_i)\,dh_i , \tag{20}$$

$$P_2 = \int_{(h-h_{cr})}^{h} p_{cr}\left(\frac{h-h_i}{l}\right)2m\pi(R-h_i)\,dh_i . \tag{21}$$

Then, we have

$$\frac{P}{P_{cr}m\pi l^2} = \varepsilon_{cr}\left(\frac{R}{l}-\frac{h}{l}+\frac{2}{3}\varepsilon_{cr}\right)+\left(\frac{h}{l}-\varepsilon_{cr}\right)\left[2\frac{R}{l}-\frac{h}{l}+\beta\frac{R}{l}\frac{h}{l}+\right.$$

$$\left.+\left(1+\beta\frac{R}{l}\right)\varepsilon_{cr}-\beta\frac{h}{l}\left(\frac{h}{l}-\varepsilon_{cr}\right)+\beta\frac{2}{3}\left(\frac{h}{l}-\varepsilon_{cr}\right)^2\right]. \tag{22}$$

For the case of $R >> l$, Eq. (22) simplifies as Eq. (19).

When $h < h_{cr}$,

$$\frac{P}{P_{cr}m\pi Rl} = \frac{1}{\varepsilon_{cr}}\left(\frac{h}{l}\right)^2 . \tag{23}$$

When $h > h_{cr}$,

$$\frac{P}{P_{cr}m\pi Rl} = \varepsilon_{cr}+\left(\frac{h}{l}-\varepsilon_{cr}\right)\left(2+\beta\frac{h}{l}\right). \tag{24}$$

Results of indentation into forests of coiled carbon nanotubes show a force–depth relationship of $F - h_2$, which accounts for the individual elastic contribution of the carbon nanotube and the contact geometry.

3. Results and Discussion. As an example, consider a spherical indenter with radius $R = 50l$ and each individual nanowire in nanowire forests having the same length, diameter, and material properties as the nanowire in Fig. 2. With these parameters and Eq. (16), a density $m < 7.77$ for pinned-fixed nanowire forests and $m < 25$ for cantilever nanowire forests can avoid adhesion instability of two neighboring nanowires.

Figures 4 and 5 compare the load–depth behavior while considering compression, buckling, and post-buckling, between the solution with surface effect and the classical solution in which surface effect is neglected. For pinned-fixed nanowire forests in Fig. 4, compared to the classical solution, the dimensionless applied load F/P_{cr}^0 accounted the surface effects are much significantly larger and trend to show a stiffer behavior when areal density $m = 7$, while the cantilever nanowire forests show the opposite trends in Fig. 5. The results show that the surface effects play an important role in depth-dependent hardness. Evidently, for the different areal densities of $m = 5$ and 7, the dimensionless applied load F/P_{cr}^0 becomes larger as the increase of m for both pinned-fixed nanowire forests and cantilever nanowire forests.

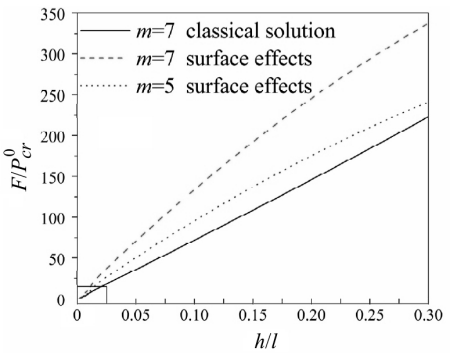

Fig. 4

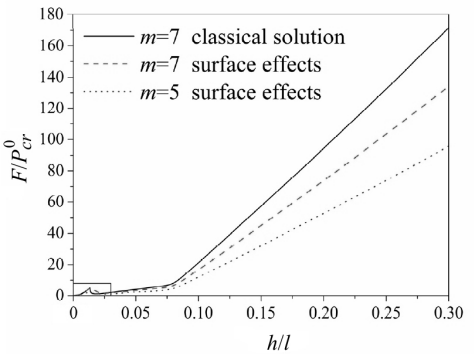

Fig. 5

Fig. 4. The load–depth behavior of pinned-fixed nanowire forests with different area densities.
Fig. 5. The load–depth behavior of cantilever nanowire forests with different area densities.

Conclusions. In this paper, the surface effects of surface elasticity and residual surface stress on mechanics of indentation into well-ordered forests of nanowires by a relatively large spherical indenter ($R >> l$) is analyzed and discussed. During the whole indentation process, the complicated deformation behavior of nanowire forest with a large-radius spherical indenter includes compression, buckling, and postbuckling. The surface effect contribute noticeably to the mechanical behavior of nanowire forests due to a remarkably large surface area/volume ratio. The surface and packing density effect on the in-depth behavior of indentation of nanowire forest is discussed. When the surface effect is allowed for, pinned-fixed nanowire forests tend to be stiffer than classical beam forests, while the cantilever case tends towards a softer behavior. The study is instrumental in measuring the mechanical properties of the nanowire forest and in designing nanowire-forest devices for various applications.

Acknowledgments. Project (11502197) supported by the National Natural Science Foundation of China; Project (2016JQ1032) supported by the Science and Technology Department of Shaanxi Province; Project (16JK1504) supported by the Education Department of Shaanxi Province; Post-doctoral program in Shaanxi Province.

1. M. Rana and M. R. Mohd Asyraf, "Investigation and development of vertically aligned carbon nanotube (VACNT) forest based temperature sensor," *Microelectron. Eng.*, **162**, 93–95 (2016).
2. M. Salado, M. Oliva-Ramirez, S. Kazim, et al., "1-dimensional TiO_2 nano-forests as photoanodes for efficient and stable perovskite solar cells fabrication," *Nano Energy*, **35**, 215–222 (2017).
3. Z. G. Zhu, L. Garcia-Gancedo, C. Chen, et al., "Enzyme-free glucose biosensor based on low density CNT forest grown directly on a Si/SiO_2 substrate," *Sensor. Actuat. B - Chem.*, **178**, 586–592 (2013).
4. M. R. Maschmann, Q. Zhang, F. Du, et al., "Length dependent foam-like mechanical response of axially indented vertically oriented carbon nanotube arrays," *Carbon*, **49**, No. 2, 386–397 (2011).
5. Z. M. Xiao, M. Dahmardeh, M. V. Moghaddam, et al., "Scaling approach toward nano electro-discharge machining: Nanoscale patterning of carbon nanotube forests," *Microelectron. Eng.*, **150**, 64–70 (2016).
6. H. J. Qi, K. B. K. Teo, K. K. S. Lau, et al., "Determination of mechanical properties of carbon nanotubes and vertically aligned carbon nanotube forests using nano-indentation," *J. Mech. Phys. Solids*, **51**, Nos. 11–12, 2213–2237 (2003).
7. L. F. Wang, C. Ortiz, and M. C. Boyce, "Mechanics of indentation into micro- and nanoscale forests of tubes, rods or pillars," *J. Eng. Mater. Technol.*, **133**, No. 1, 011014 (2011).
8. C. Q. Chen, Y. Shi, Y. S. Zhang, et al., "Size dependence of Young's modulus in ZnO nanowires," *Phys. Rev. Lett.*, **96**, No. 7, 075505 (2006).
9. R. E. Miller and V. B. Shenoy, "Size-dependent elastic properties of nanosized structural elements," *Nanotechnology*, **11**, No. 3, 139–147 (2000).
10. G. F. Wang and X. Q. Feng, "Effects of surface elasticity and residual surface tension on the natural frequency of microbeams," *Appl. Phys. Lett.*, **90**, No. 23, 231904 (2007).
11. G. F. Wang and X. Q. Feng, "Surface effects on buckling of nanowires under uniaxial compression," *Appl. Phys. Lett.*, **94**, No. 14, 141913 (2009).
12. J. He and C. M. Lilley, "Surface effects on the elastic behavior of static bending nanowires," *Nano Lett*., **8**, 1798–1802 (2008).
13. K. W. Qiu, Y. Lu, D. Y. Zhang, et al., "Mesoporous, hierarchical core/shell structured $ZnCo_2O_4/MnO_2$ nanocone forests for high-performance supercapacitors," *Nano Energy*, **11**, 687–696 (2015).
14. X. P. Zheng, Y. P. Cao, B. Li B, et al., "Surface effects in various bending-based test methods for measuring the elastic property of nanowires," *Nanotechnology*, **21**, No. 20, 1719–1742 (2010).
15. R. C. Cammarate, "Surface and interface stress effects in thin films," *Prog. Surf. Sci*., **46**, No. 1, 1–38 (1994).
16. N. Challamel and I. Elishakoff, "Surface elasticity effects can apparently be explained via their non-conservativeness," *J. Nanotechnol. Eng. Med.*, **2**, No. 3, 031008 (2011).
17. G. F. Wang and F. Yang, "Postbuckling analysis of nanowires with surface effects," *J. Appl. Phys.*, **109**, 063535 (2011).

Received 15. 09. 2017